Supporting Information

Charge Separation and Triplet Exciton Formation Pathways in Small Molecule Solar Cells as Studied by Time-resolved EPR Spectroscopy

Stuart A. J Thomson[§], Jens Niklas[‡], Kristy L. Mardis[†], Christopher Mallares[†], Ifor D. W Samuel[§] & Oleg G. Poluektov[‡]

§ Organic Semiconductor Centre, SUPA, School of Physics & Astronomy, University of St Andrews, St Andrews KY16 (SS, UK

† Department of Chemistry and Physics, Chicago State University, Chicago, Illinois 60628, USA

‡Chemical Sciences and Engineering Division, Argonne National Laboratory, Argonne, Illinois 60439, USA

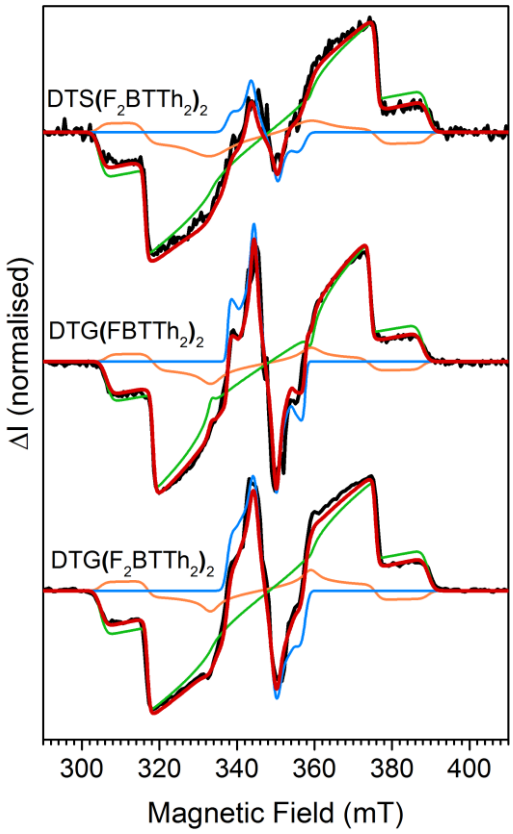

Figure S1: Continous wave direct detection TR-EPR triplet exciton spectra of fluorobenzothiadiazole donors blended with $PC_{61}BM$ in frozen chlorobenzene solution at T = 50 K. Spectra were captured 500 ns after the laser flash. Positive peaks correspond to absorption (A) and negative to emission (E). The experimental spectra (black) are shown alongside theoretical simulations of the ISC triplet exciton residing on the donor (green), BET triplet exciton residing on the donor (orange), ISC triplet exciton residing on $PC_{61}BM$ (blue) and the superposition of these (red).

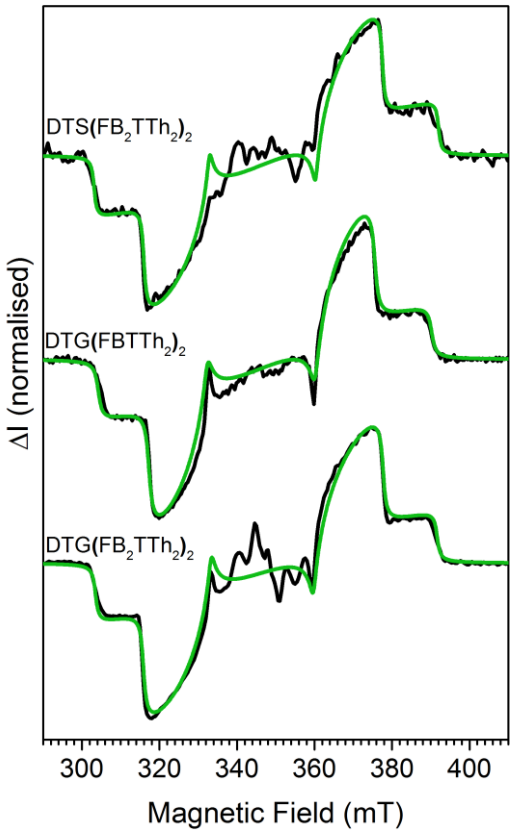

Figure S2: Continous wave direct detection TR-EPR triplet exciton spectra of solution cast films of fluorobenzothiadiazole donors blended with $PC_{61}BM$ at T = 50 K. Spectra were captured 500 ns after the laser flash. Positive peaks correspond to absorption (A) and negative to emission (E). The experimental spectra (black) are shown alongside theoretical simulations of the ISC triplet exciton residing on the donor (green), assuming partial orientation.

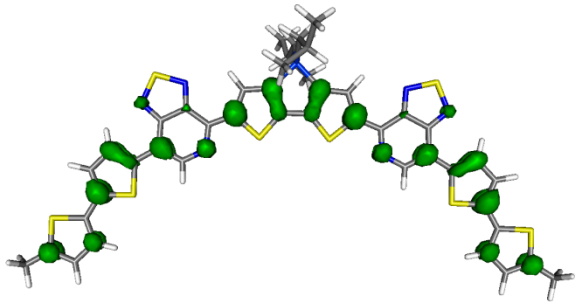

a

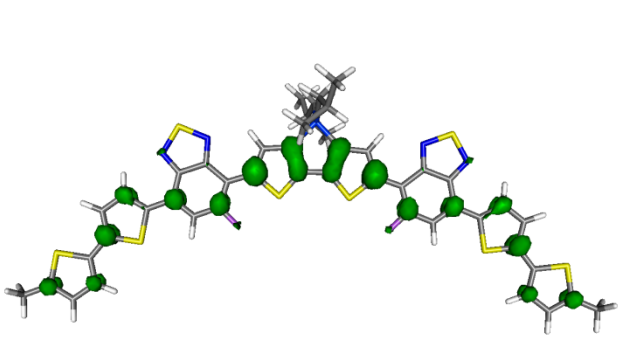

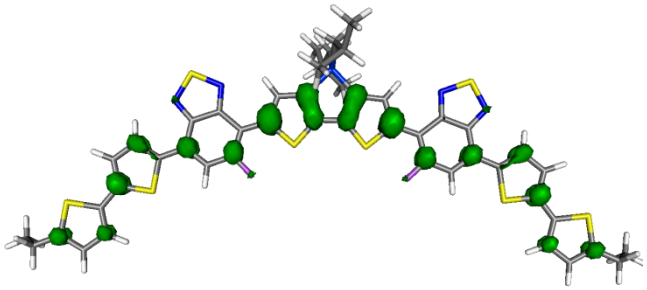

b

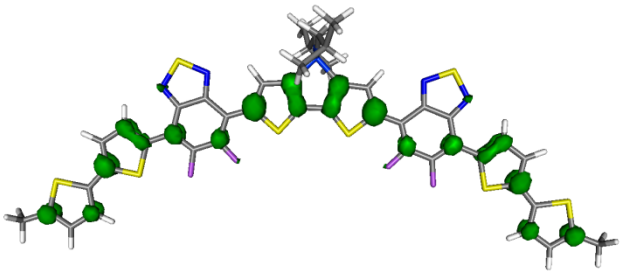

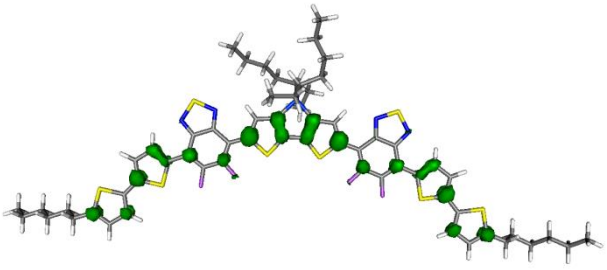

c

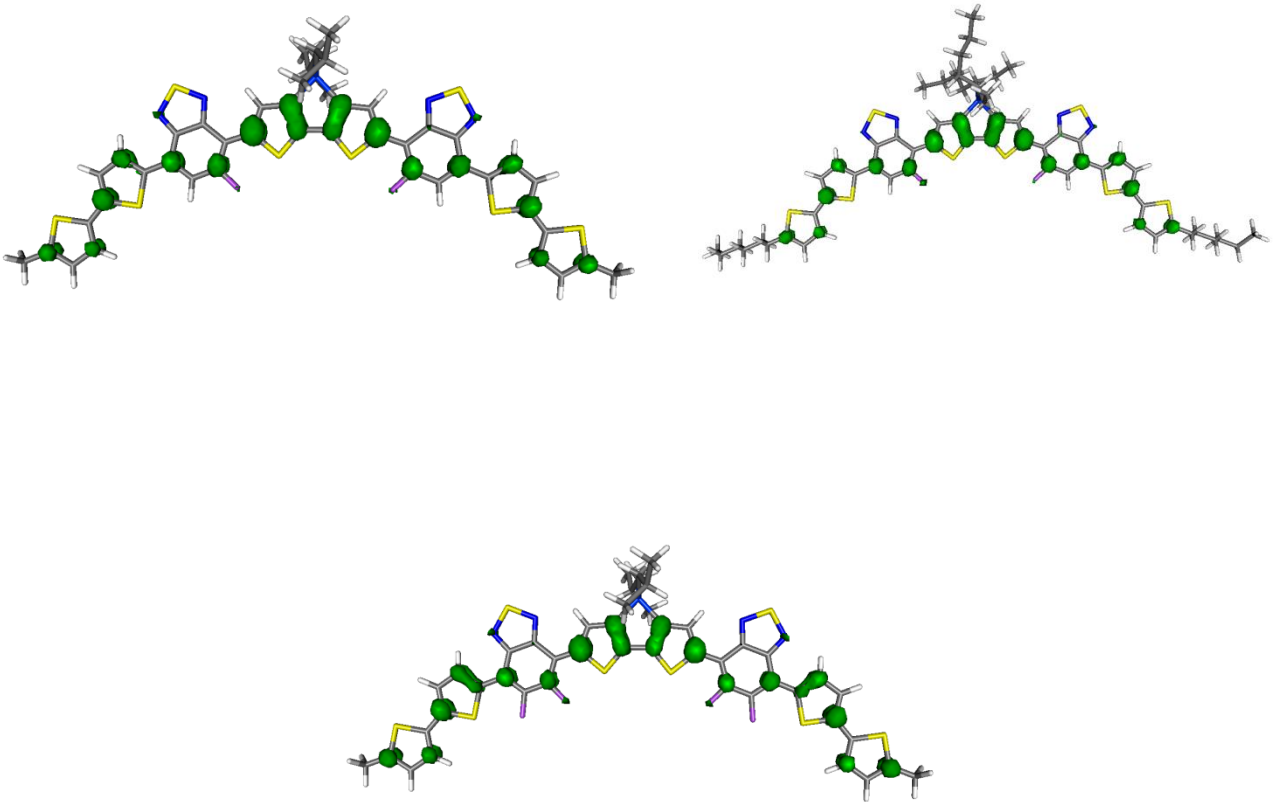

Figure S3. Spin density isosurface plots at a 0.002 e/a_0^3 level of optimized (B3LYP|6-31G*) model structures for the cation radicals a) DTS($PTTh_2$)$_2$; b) DTS($FBTTh_2$); c) DTS(F_2BTTh_2); d.) DTG($FBTTh_2$); e) DTG(F_2BTTh_2)$_2$. The two structures in b, c, and d just differ in the alkyl substituents on the X and the thiophene.

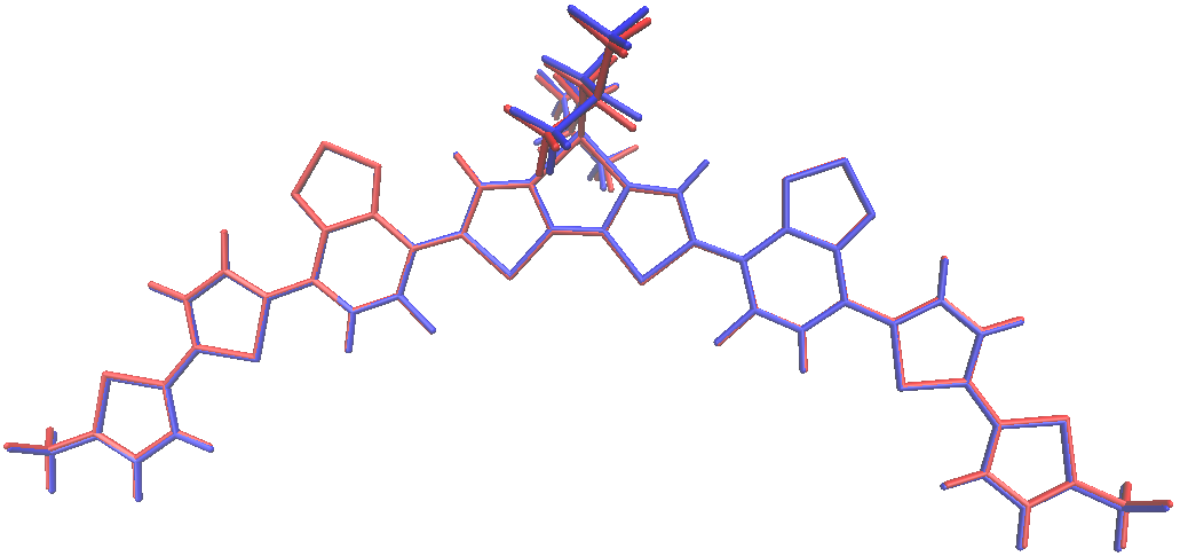

Figure S4. Overlay of DTS(FBTTh$_2$)$_2$ (red) and DTG(FBTTh$_2$)$_2$ (blue). The RMSD is less than 0.5 Å.

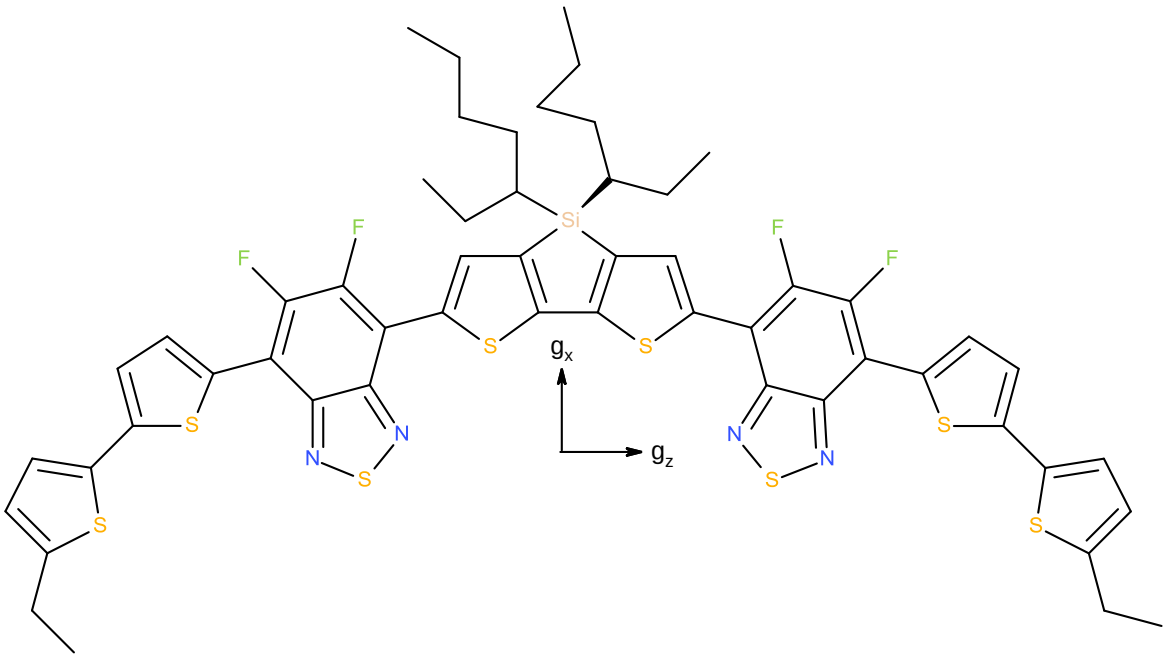

Figure S5. Orientation of the g-tensor axes on the monomer units. The g_y tensor axis is perpendicular to the other two (out of the plane of the figure). The orientation is the same for all monomers.

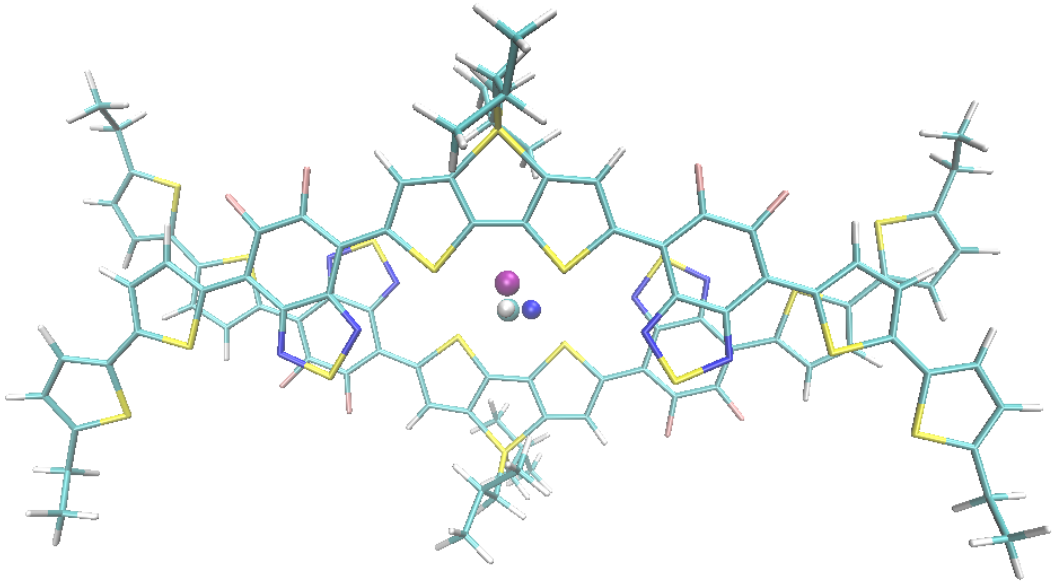

Figure S6. Orientation of the g-tensor axes in the DTS(F_2BTTh$_2$) dimer. The g_y tensor axis is perpendicular to the other two (out of the plane of the figure; white to cyan). As in the monomer, g_z (white to blue) is still directed along the backbone, g_x (white to magenta) perpendicular in the plane, and g_y lies along the axis that connects the two units.

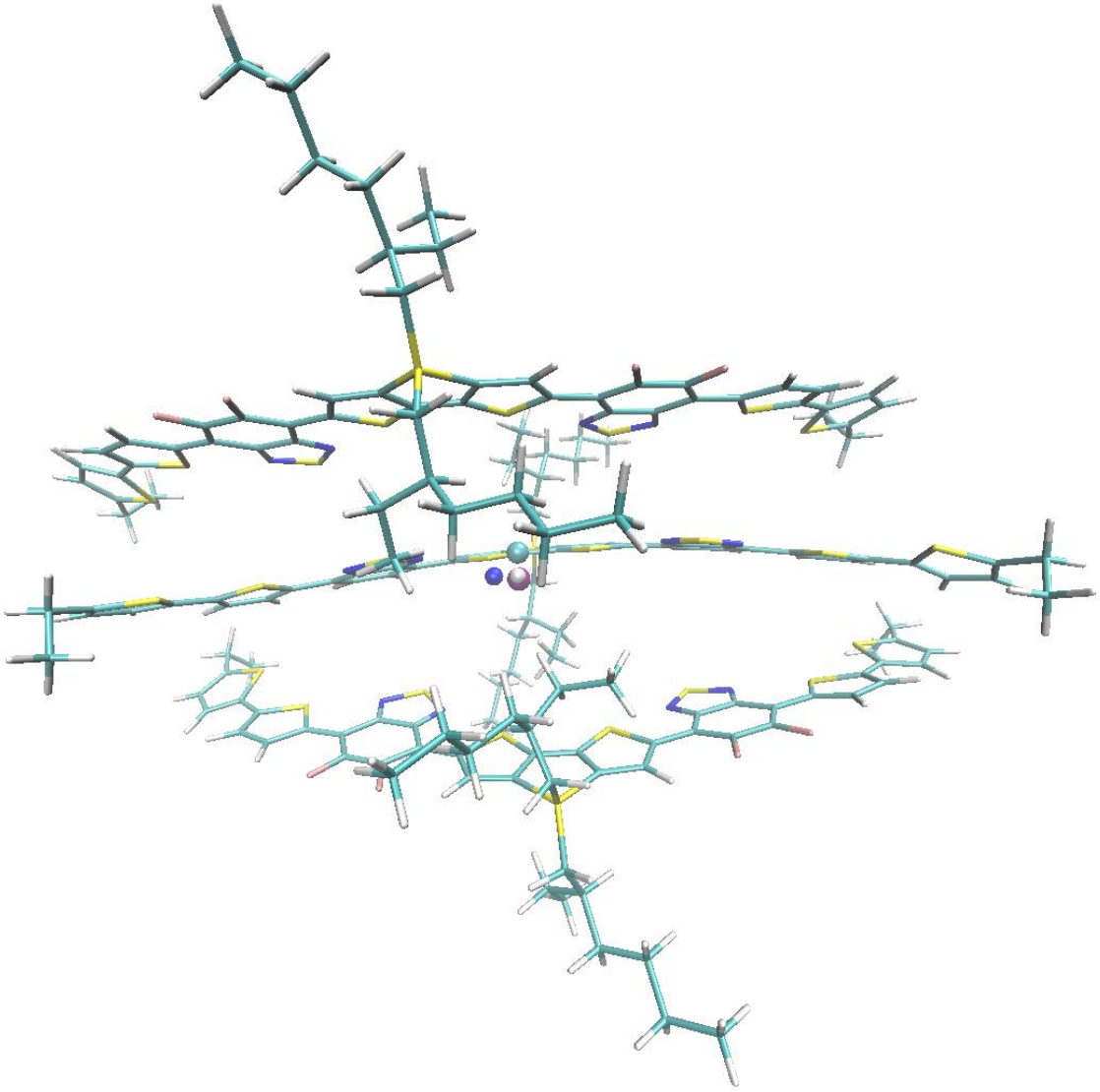

Figure S7. Orientation of the g-tensor axes for the DTS(F_2BTTh$_2$) trimer. As in the monomer, the trimer g_z axis is directed along the backbone, g_x (white to magenta) perpendicular in the plane, and g_y lies along the axis connecting the two units (white to cyan).

Table S1. Comparison of calculated g-values on central substituent, thiophene substituent, and conformation. The cis/trans conformations are defined in terms of the sulfur atoms.

Molecule	Central Substituent	Thiophene Alkyl Substituent	Conformation*	g_1	g_2	g_3
DTS(PTTh$_2$)$_2$	isopropyl	ethyl	TTTTTT	2.0012	2.0023	2.0025
	isopropyl	methyl	TTTTTT	2.0015	2.0021	2.0023
	isopropyl	methyl	TTCCTT	2.0008	2.0023	2.0029
DTS(FBTTh$_2$)$_2$	isopropyl	methyl	TTTTTT	2.0012	2.0023	2.0025
	isopropyl	ethyl	TTTTTT	2.0012	2.0023	2.0025
	isopropyl	methyl	TTCCTT	2.0008	2.0023	2.0029
DTS(F$_2$BTTh$_2$)	isopropyl	methyl	TTTTTT	2.0012	2.0023	2.0023
	2-methyl hexyl	ethyl	CCCCCC	2.0002	2.0024	2.0034
DTG(FBTTh$_2$)	isopropyl	methyl	TTTTTT	2.0011	2.0024	2.0025
	hydrogen	hydrogen	TCTCCT	2.0007	2.0025	2.0026
DTG(F$_2$BTTh$_2$)	isopropyl	methyl	TTTTTT	2.0010	2.0023	2.0025

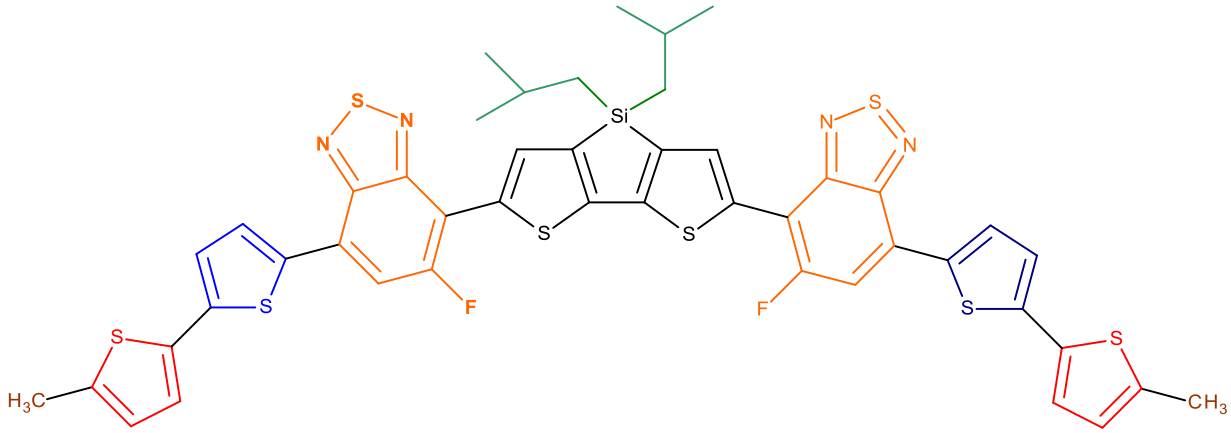

Table S2. Isotropic hyperfine coupling constants (MHz) of ^{1}H calculated using DFT (B3LYP||EPRII||def2-TZVPP) for the five model compounds. The values for the unfluorinated DTS(PTTh$_2$)$_2$ are significantly larger than those on either the mono or di-fluorinated complexes which are all very similar to each other. The first value is the hydrogen closest to the center in a given pair. For the dimer and trimer the rows correspond to each constituent molecule. Color coding with reference to the schematic structure shown above.

Molecule	central unit	FBT/TP	Thiophene 1 HFC	Thiophene 2 HFC
DTS(PTTh$_2$)$_2$	0.7	-0.16	-4.7/-0.9	-4.17/0.30
DTS(FBTTh$_2$)$_2$	-0.3	1.29	-3.8/-0.4	-3.1/.25
DTG(FBTTh$_2$)	-0.3	1.41	-3.9/-0.3	-3.1/0.3
DTG(F$_2$BTTh$_2$)	-0.2	----	-3.8/-0.87	-3.7/0.24
DTS(F$_2$BTTh$_2$)	-0.2	----	-3.8/-0.9	-3.7/.23
Dimer	-.3/-.2	----	-1.6/-.5	-1.8/.2
DTS(F$_2$BTTh$_2$)	-.3/-.2		-1.8/-.5	-1.7/.2
Trimer	-.1/-.1	----	-.9/-.2	-.9/.1
DTS(F$_2$BTTh$_2$)	-.3/-.1		-1.3/-.2	-1.3/.1
	-.2/-.1		-1.3/-.3	-1.3/.2

Table S3. Mulliken Spin Populations. The functional units are the same as those shown in the schematic structure shown above Table S2.

Group	DTS(FBTTh$_2$)$_2$	DTS(PTTh$_2$)$_2$
dithienosilole	0.45	0.35
Silicon	-0.01	-0.01
FBT/PT	0.19	0.14
thiophene 1	0.22	0.31
thiophene 2	0.14	0.20
Si alkyl	0.00	-0.00
alkyl	0.004	0.005
total	0.99	1.00

Table S4. Comparison of calculated g-values for DTS(FBTTh$_2$)$_2$ as a function of the functional used during optimization. All structures used the 6-31G* basis set and were all trans conformation with the ethyl substituent on the thiophene and 2-ethylhexyl on the silicon.

Functional	g_z	g_y	g_x
B3LYP	2.0012	2.0022	2.0025
BP	2.0011	2.0023	2.0024
CAM-B3LYP	2.0008	2.0023	2.0024
TPSSH	2.0016	2.0023	2.0025
ωB97X	2.0010	2.0023	2.0025

Table S5. Calculated ^{19}F hyperfine coupling constants (MHz). A1, A2, and A3 are the principal values of the hyperfine tensor. For DTS(F_2BTTh$_2$)$_2$, the larger value in each pair is for the fluorine that is closer to the center of the molecule.

	A_1	A_2	A_3	A_{iso}
DTS(FBTTh$_2$)$_2$	-3.0	-7.3	+32.2	+7.3
	-2.9	-7.3	+32.2	+7.3
DTS(F_2BTTh$_2$)$_2$	+0.4	+1.8	-14.2	-4.0
	-2.2	-5.7	+26.2	+6.1
	+0.4	+1.8	-14.1	-4.0
	-2.1	-5.6	+25.8	+6.0

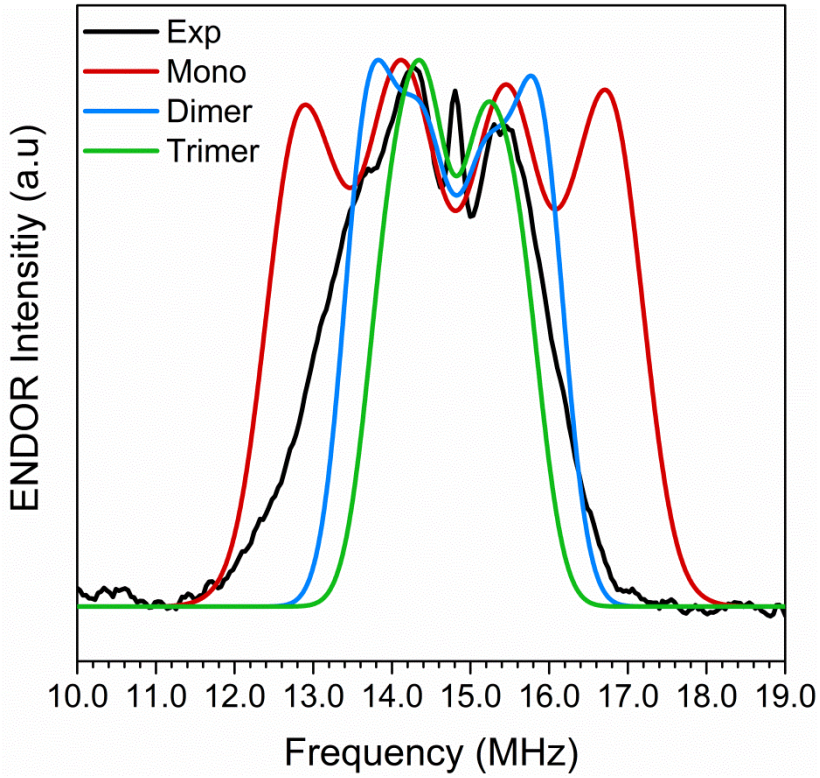

Figure S8. ENDOR spectra of DTS(F_2BTTh$_2$)$_2$. The experimental spectrum is shown in black and was measured from a frozen solution of DTS(F_2BTTh$_2$)$_2$:PC_{61}BM at 50 K using the Mims pulse sequence. ^1H simulations (using the hyperfine parameters obtained from the DFT

calculations) of the monomer, dimer, and trimer are shown red, blue and green respectively. The Mims pulse sequence has periodic blind spots including one in the center, which results in a suppression of the weak hyperfine couplings.[1-2] The simulated spectra were therefore treated with a function to mimic the experimental suppression effects.[2] In addition the simulations were broadened using a Gaussian distribution to imitate the distribution in in hyperfine values (AStrain) that would be present in the sample. Looking at the high frequency side of the spectrum, so as to not be influenced by the ^{19}F coupling, it is clear that that mono simulation severely overestimates the width of the spectrum. This overestimation occurs even with no broadening (AStrain) included in the simulation. In comparison the simulations of the dimer and trimer reproduce the experimental width much more favorably.

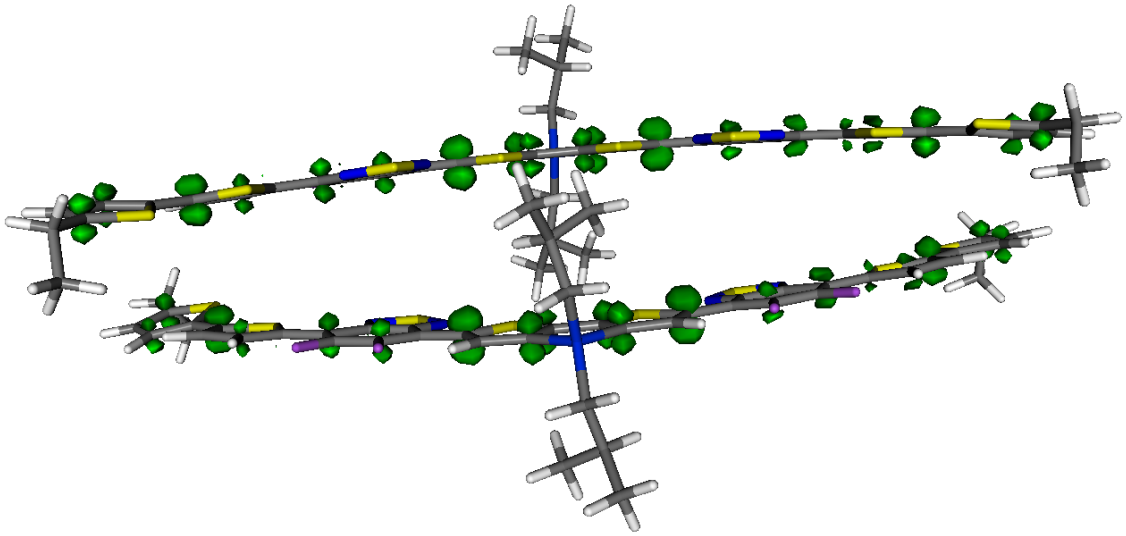

a

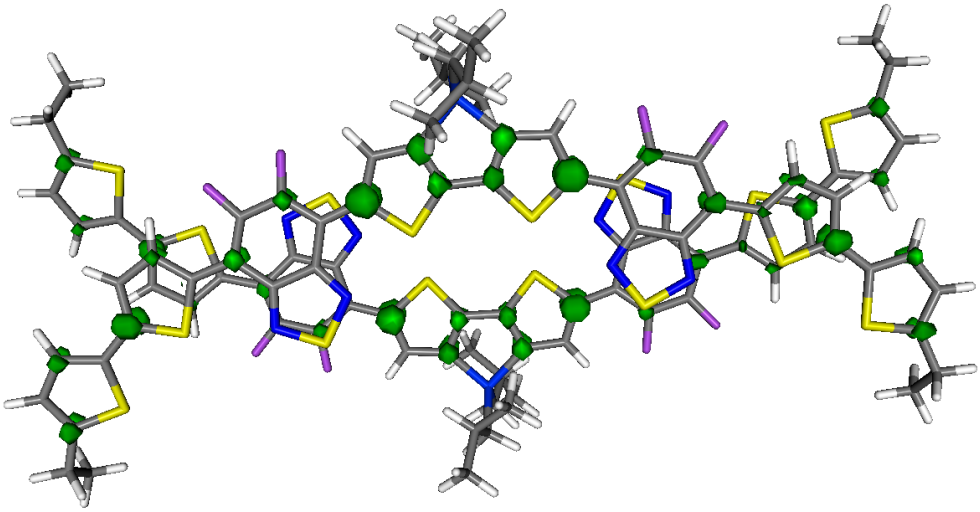

b

Figure S9. Side (a) and top (b) views of DTS(FB_2TTh_2)$_2$ dimer with an overall +1 charge showing spin density isosurface at 0.001 e/a_0^3.

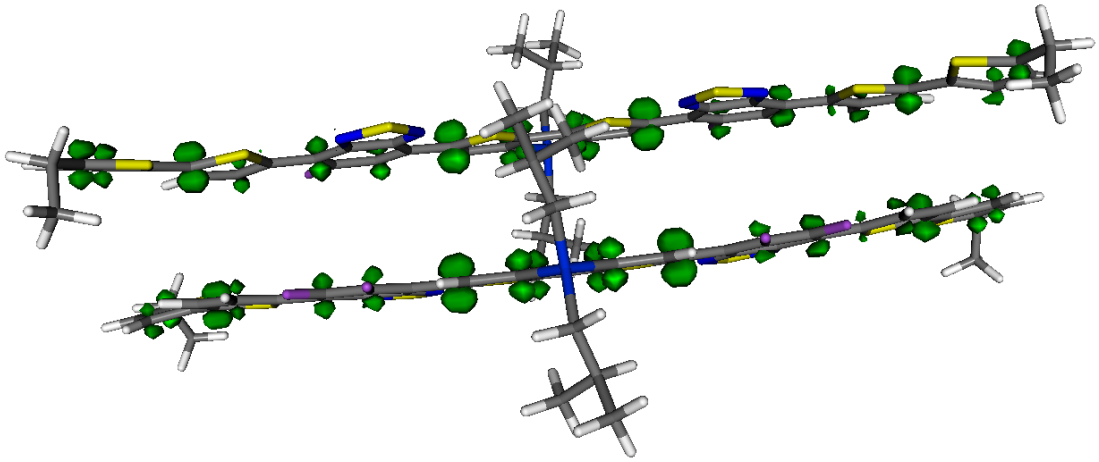

a

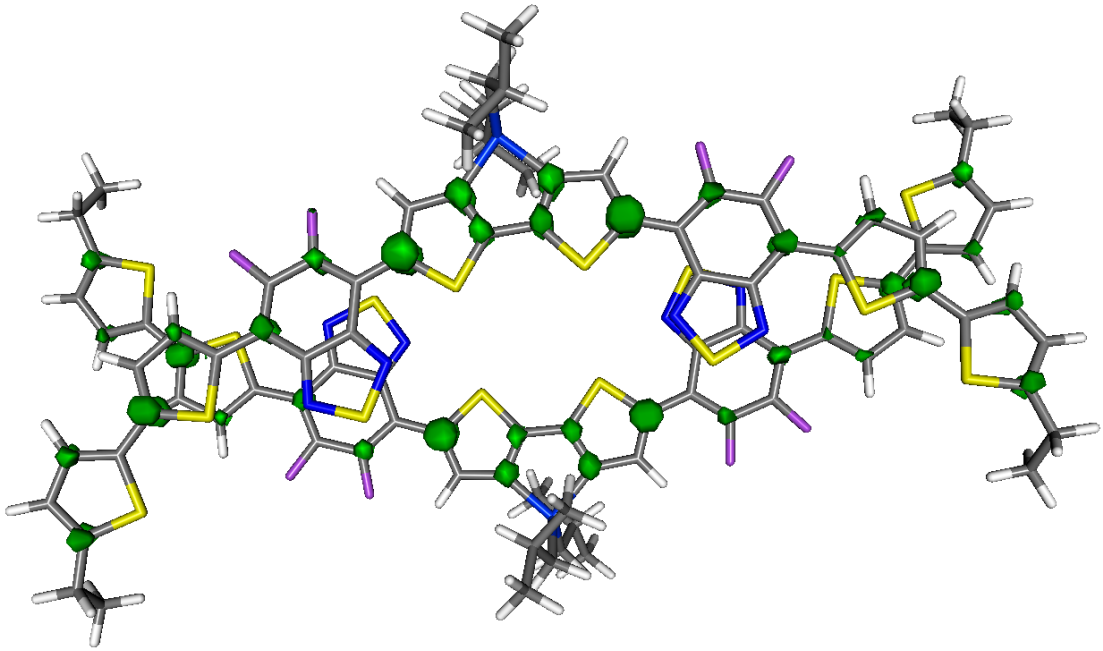

b

Figure S10. Side (a) and top (b) views of DTG(FB_2TTh_2)$_2$ dimer with an overall +1 charge showing spin density isosurface at 0.001 e/a_0^3.

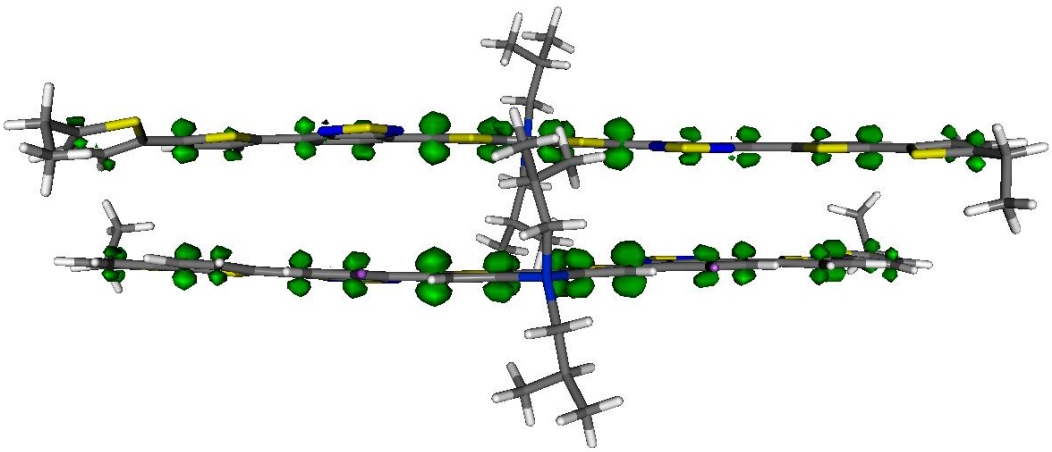

a

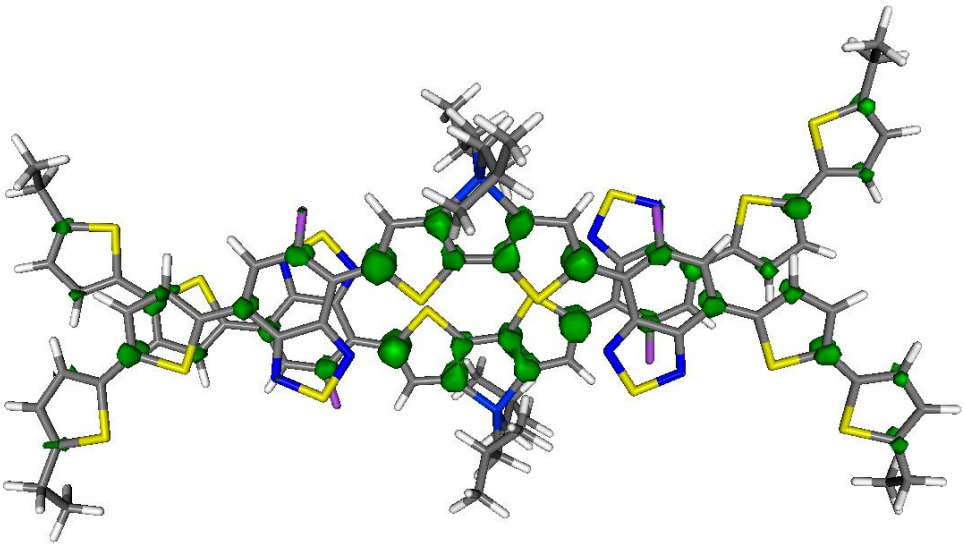

b

Figure S9. Side (a) and top (b) views of DTS(FBTTh$_2$)$_2$ dimer with an overall +1 charge showing spin density isosurface at 0.001 e/a_0^3.

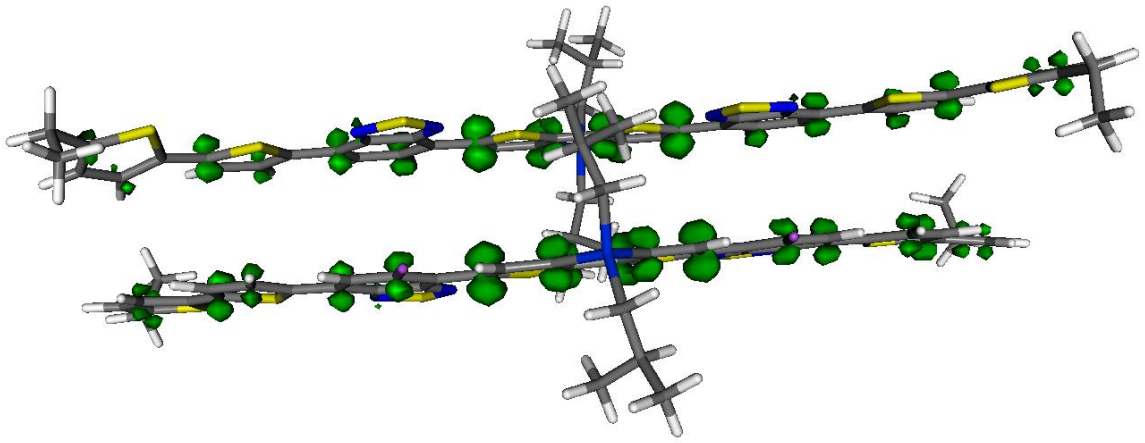

a

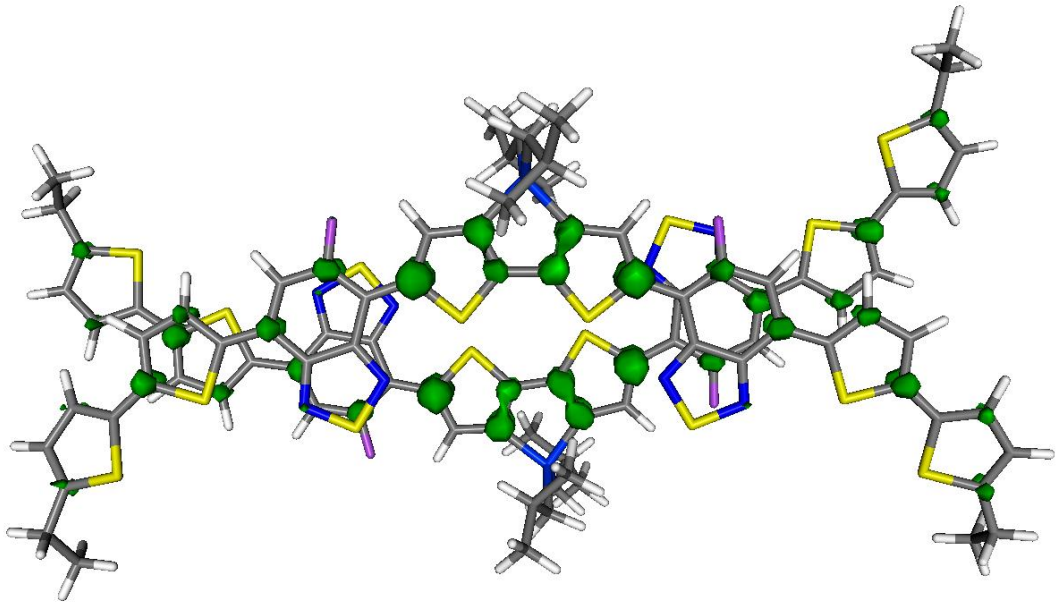

b

Figure S10. Side (a) and top (b) views of DTG(FBTTh$_2$)$_2$ dimer with an overall +1 charge showing spin density isosurface at 0.001 e/a_0^3.

1. Gemperle, C.; Schweiger, A., Pulsed electron nuclear double-resonance methodology. *Chem. Rev.* **1991,** *91* (7), 1481-1505.
2. Doan, P. E.; Lees, N. S.; Shanmugam, M.; Hoffman, B. M., Simulating suppression effects in pulsed endor, and the 'hole in the middle' of mims and davies endor spectra. *Appl. Magn. Reson.* **2010,** *37* (1-4), 763-779.